Review of Computer Engineering Research
2026 Vol. 13, No. 2, pp. 49-66
ISSN(e): 2410-9142
ISSN(p): 2412-4281
DOI: 10.18488/76.v13i2.4982

FEARE: A fuzzy entropy-driven adaptive region energy active contour model for medical image segmentation

Sivakumar Kaliyappan[1+]
Bhoopathy Bagan K[2]

[1]*Department of Electronics and Communication Engineering, Panimalar Engineering College, Chennai, Tamil Nadu, India.*
[1]*Email: ksivakumar.ece@panimalar.ac.in*
[2]*Department of Electronics Engineering MIT Campus, Chromepet, Anna University, Chennai, India.*
[2]*Email: bhoopathy02@yahoo.com*

(+ Corresponding author)

Article History
Received: 10 November 2025
Revised: 2 March 2026
Accepted: 16 April 2026
Published: 29 May 2026

Keywords
Active contour model
Cardiac MRI
Fuzzy entropy
Medical image segmentation
Region-based energy.

ABSTRACT

Image segmentation plays a critical role in medical image analysis, where intensity inhomogeneity, noise, and weak boundaries often degrade performance. Many region-based active contour models rely on fixed assumptions, limiting their adaptability in complex clinical scenarios. To address this limitation, we propose FEARE, a fuzzy entropy-driven adaptive region energy active contour model within a level-set framework. The model incorporates entropy-guided confidence weighting to dynamically adjust region fitting in uncertain regions, while a geometry-aware regularization term preserves anatomical plausibility during contour evolution. The proposed method is evaluated on the Sunnybrook Cardiac MRI dataset using overlap, boundary, and efficiency metrics. FEARE achieves a mean Dice Similarity Coefficient of 0.846 and an Intersection over Union of 0.757, outperforming several state-of-the-art active contour models with fewer segmentation failures, while maintaining competitive computational efficiency. These results demonstrate that entropy-driven adaptive modeling improves segmentation robustness without requiring training data. The FEARE framework provides an interpretable and data-efficient alternative to learning-based methods for medical image segmentation. The evaluation scripts and source code are publicly available to make them reproducible. The FEARE model's source code is available at https://doi.org/10.5281/zenodo.1555982, and the Sunnybrook Cardiac MRI dataset is available at https://www.cardiacatlas.org/sunnybrook-cardiac-data/.

Contribution/Originality: This study contributes to the existing literature by introducing a fuzzy entropy-driven adaptive region energy model for medical image segmentation. This study uses entropy-based confidence weighting to dynamically modulate region fitting. This study originates a unified variational formulation integrating entropy and geometry-aware regularization, improving robustness under uncertainty.

1. INTRODUCTION

Medical image segmentation plays a pivotal role in computer-aided diagnosis, treatment planning, and clinical research by enabling the extraction of anatomically significant structures from complex visual data [1]. Accurate segmentation remains a major challenge due to inherent noise, intensity inhomogeneity, texture variation, and blurred boundaries that are commonly present in modalities such as MRI and CT [2, 3]. These difficulties are further exacerbated in pathological regions that exhibit irregular shapes or uncertain structural boundaries.

Active contour models (ACMs) have emerged as a powerful class of methods that evolve deformable curves to delineate object boundaries based on variational energy formulations [4, 5]. Classical models such as Chan and Vese

[4], Local Binary Fitting (LBF) [6], and other localized region-based formulations have demonstrated notable segmentation accuracy under certain assumptions. However, they typically suffer from sensitivity to intensity non-uniformity, low-contrast boundaries, and high noise interference.

To overcome these issues, fuzzy region-based models have been proposed to incorporate uncertainty modeling into the contour evolution process [7-9]. These methods provide robustness against noise and weak gradients but often employ fixed uncertainty structures that limit their adaptability across diverse image contexts. Similarly, entropy-based energy formulations have been employed to enhance region modeling under ambiguity, while recent hybrid models integrate local-global terms or region-edge energy to improve convergence in complex scenes [10, 11]. Despite these advances, existing models still lack a flexible mechanism that dynamically adapts the energy fitting behaviour based on local structural ambiguity, while preserving anatomical shape information during evolution.

To address these limitations, a novel segmentation framework termed FEARE (Fuzzy Entropy Adaptive Region Energy) is introduced. FEARE integrates fuzzy entropy weighting into a local fitting term to adaptively control energy contributions in uncertain regions. In addition, a structural conformity regularization term is incorporated to preserve the plausibility of the evolving contour, even in noisy or pathological environments. The resulting energy formulation is embedded within a level-set framework, yielding a unified variational model that simultaneously achieves robustness and shape-aware segmentation.

To validate its performance, FEARE is tested on the Sunnybrook Cardiac MRI dataset [12], which contains four pathological heart conditions. Comparative analysis is performed against nine state-of-the-art active contour methods [4, 8-10, 13, 14] using a comprehensive evaluation suite that covers overlap accuracy (Dice Similarity Coefficient, Intersection over Union), boundary accuracy (Average Perpendicular Distance, Mean Absolute Deviation, Hausdorff Distance, Fourier Distance), and efficiency (execution time, memory usage) [4, 8-10, 13]. In response to persistent gaps, non-adaptive uncertainty handling, and insufficient shape preservation, we introduce FEARE, which couples entropy-driven confidence weighting with local region fitting and geometry-aware regularization to maintain anatomical plausibility under noise and inhomogeneity.

We propose an entropy-adaptive region energy formulation to improve active contour segmentation in the presence of local uncertainty. The framework employs a fuzzy entropy-based estimation strategy to moderate locally imposed region fitting within a level-set formulation, leading to adaptive behavior when regions are spatially uncertain. The approach avoids the fixed uncertainty handling of traditional region-based active contour models and is explicit in its consideration of uncertainty-based adaptivity and integrates entropy weighting with geometry-aware regularization in a unified variational framework. It offers a principled mechanism to enhance segmentation robustness while remaining fully training-free. Experiments on cardiac MRI data show the performance gains to be robust with a broad range of pathological cases and validate the efficacy of entropy-guided adaptation in challenging clinical imaging situations.

The remainder of this paper is organized as follows. Section 2 discusses related work. Section 3 presents the proposed method. Section 4 reports the experimental results and discussion. Section 5 provides the ablation study on entropy weighting and sigmoid scaling parameters. Section 6 presents the qualitative comparison of segmentation results. Section 7 discusses limitations and future directions. Section 8 concludes the study.

2. RELATED WORK

Active contour models (ACMs) have long been central to medical image segmentation due to their ability to evolve contours under data-driven forces within a variational framework. Early works, such as the Snakes model [5], introduced the idea of minimizing internal and external energies for contour evolution. Later, edge-based geodesic models [15, 16] leveraged gradient information to better align with object boundaries but suffered from poor performance in regions with weak edges or high noise. Region-based models like the Chan and Vese [4] marked a transition toward statistical/local region modeling that better handles intensity inhomogeneity. These models,

however, often underperform when faced with inhomogeneous or textured regions due to their reliance on uniform region assumptions.

To improve robustness under intensity variation, localized models such as Local Binary Fitting (LBF) introduced region-specific statistics into the energy formulation. Although these models handle local inhomogeneities more effectively, they remain sensitive to parameter tuning and often lack mechanisms to adapt to structural uncertainty.

Fuzzy logic–based models were introduced to better handle ambiguity in region boundaries. The Fuzzy Active Contour Models (FACMs) proposed by Fang, et al. [7]; Fang, et al. [8] and Fang, et al. [9] integrated global and local fuzzy energy into the level-set formulation, enabling more adaptive region control. Hybrid models, such as those combining region and edge forces [9] and patch-based pressure functions [10], further improved segmentation under noisy and low-contrast conditions. Recently, Meng and Si [13] proposed a hybrid signed pressure force (SPF) model, enhancing performance on complex anatomical structures, while Ma, et al. [11] proposed adaptive local-fitting-based ACMs specifically targeting medical images. Very recent TVC work further strengthens edge cues through anisotropic, edge-enhanced active contours driven by difference-of-Gaussian (DoG) filtering, improving robustness across categories [17].

Entropy-based models like the Edge Entropy Fitting (EEF) model and the Optimized Laplacian of Gaussian (LoG) energy model [2] incorporated statistical uncertainty into the contour evolution process. Although entropy improves uncertainty handling, these models apply entropy uniformly across the image without distinguishing between low- and high-confidence regions. Moreover, many existing models lack shape-preserving mechanisms, which is particularly critical for medical structures where anatomical conformity is important.

Deep learning–based methods such as U-Net [18] and its extensions [19, 20] have significantly advanced segmentation accuracy, particularly in large datasets. However, such models demand extensive annotated training data and remain largely black-box in nature, raising concerns about explainability and robustness in clinical deployment [21, 22]. While they offer superior performance in many cases, their use in situations with limited labeled data or high interpretability requirements remains limited. In this context, explainable machine learning frameworks [23] and hybrid approaches that combine mathematical models with learned priors have emerged [20, 24] yet still struggle with generalizability across different pathologies. On the learning side, TVC has reported semi-supervised pipelines that combine imbalanced pseudo-label filtering with nnU-Net enhancement, yielding stronger performance under scarce labels [25].

Despite these numerous advancements, the challenges of spatial uncertainty, texture-induced region confusion, and structure preservation remain only partially addressed. The existing models often treat image regions uniformly, failing to adaptively modulate energy influence based on local fuzziness or entropy. Furthermore, only a few approaches integrate entropy modeling with anatomical shape–preserving regularization. This motivates the proposed FEARE model, which introduces a fuzzy entropy adaptive fitting energy combined with a structure-aware regularization term. The aim is to dynamically adjust contour evolution in uncertain regions while maintaining anatomical plausibility across diverse pathologies. The performance of FEARE is rigorously evaluated on the Sunnybrook Cardiac dataset [12]. Using a comprehensive set of quantitative metrics, including DSC, IoU, HD, boundary distances, and efficiency, FEARE consistently outperforms nine state-of-the-art active contour models.

3. PROPOSED FEARE MODEL

The proposed FEARE (Fuzzy Entropy–Driven Adaptive Region Energy) model is formulated as a variational active contour framework in which region-based energy contributions are adaptively modulated according to local image uncertainty. Unlike conventional region-based active contour models that rely on fixed statistical assumptions, FEARE employs entropy-derived confidence weights to regulate contour evolution in spatially non-uniform or ambiguous regions. In addition, a geometry-aware regularization term is incorporated to preserve shape consistency

and anatomical plausibility during contour evolution. The formulation remains fully interpretable within the classical level-set paradigm and does not depend on training data or learned priors.

FEARE integrates three key components within a unified energy-minimization framework:

(i) local statistical fitting using Gaussian-windowed intensity means inside and outside the evolving contour.

(ii) entropy-driven confidence weighting that adaptively balances region forces based on local uncertainty.

(iii) geometry-aware regularization that enforces smooth and anatomically consistent boundaries.

Let Ω denote the image domain, $I:\Omega \to R$ the gray-scale image, and $\phi:\Omega \to R$ the level-set function whose zero level set, $C = \{x \in \Omega \mid \phi(x) = 0\}$, represents the evolving contour. The regularized Heavisine function $H_\epsilon(\cdot)$ and its derivative $\delta_\epsilon(\cdot)$ are used to define interior and exterior regions.

$$H_\epsilon(z) = \frac{1}{2}\left(1 + \frac{2}{\pi}\arctan\left(\frac{z}{\epsilon}\right)\right), \delta_\epsilon(z) = \frac{d}{dz}H_\epsilon(z) = \frac{1}{\pi}\cdot\frac{\epsilon}{\epsilon^2 + z^2}$$

The geometric regularity of the evolving contour is characterized by its curvature $\kappa(\phi)$, which is expressed in terms of second-order spatial derivatives of the level-set function.

$$\kappa(\phi) = \nabla \cdot \left(\frac{\nabla\phi}{|\nabla\phi|}\right) \quad (1)$$

To model local neighborhood interactions, a Gaussian kernel with a bandwidth σ is employed. The spatial weighting function used to define localized neighborhoods is:

$$G_\sigma(x) = \frac{1}{2\pi\sigma^2}\exp\left(-\frac{|x|^2}{2\sigma^2}\right) \quad (2)$$

The kernel is normalized by its local mass in all subsequent averages to avoid boundary bias near image borders.

3.1. Local Statistics with Gaussian Weighting

Using the Gaussian window defined in (2), FEARE computes localized intensity statistics inside and outside the evolving contour. Specifically, for each pixel $x \in \Omega$, the local class means $c_1(x)$ (inside) and $c_2(x)$ (outside) are computed as:

$$c_1(x) = \frac{\int_\Omega G_\sigma(x-y)I(y)H_\epsilon(\phi(y))dy}{\int_\Omega G_\sigma(x-y)H_\epsilon(\phi(y))dy}, c_2(x) = \frac{\int_\Omega G_\sigma(x-y)I(y)(1-H_\epsilon(\phi(y)))dy}{\int_\Omega G_\sigma(x-y)(1-H_\epsilon(\phi(y)))dy} \quad (3)$$

Based on these local class means, the fitting residuals that quantify deviations from the regional statistics are formulated as:

$$e_1(x) = (I(x) - c_1(x))^2, e_2(x) = (I(x) - c_2(x))^2 \quad (4)$$

3.2. Entropy-Driven Confidence Weighting

To quantify local uncertainty within each Gaussian neighborhood, a Shannon entropy measure is computed from the local intensity histogram. The entropy associated with the neighborhood centered at the pixel x is defined as:

$$E(x) = -\sum_{k=1}^{L} p_k(x)\log\left(p_k(x) + \varepsilon\right) \quad (5)$$

Where $p_k(x)$ denotes the probability of the intensity level k within the local histogram, L is the number of gray-level bins, and ε is a small constant introduced for numerical stability. For scale invariance, the entropy is normalized by the maximum possible entropy, yielding the normalized entropy.

$$\hat{E}(x) = \frac{E(x)}{\log L} \quad (6)$$

The normalized entropy $\hat{E}(x) \in [0,1]$ is then mapped to a confidence modulation factor. In practice, a sigmoid function controlled by a slope parameter γ and amplitude α is used, such that high entropy (ambiguous texture) yields larger modulation, while low entropy (homogeneous regions) results in smaller modulation.

3.3. FEARE Energy Functional

The FEARE framework integrates entropy-adaptive region fitting with geometric regularization into a unified variational formulation. The total energy functional to be minimized is:

$$E(\phi) = E_{\text{fit}}(\phi) + \lambda E_{\text{reg}}(\phi) \tag{7}$$

where $\lambda > 0$ is a regularization parameter. The data fidelity component explicitly embeds the entropy-derived confidence weights into the local fitting terms.

$$\varepsilon_{\text{fit}}(\phi) = \int_{\Omega}\left[(1 + \alpha\hat{E}(x))e_1(x)H_{\epsilon}(\phi(x)) + (1 - \alpha\hat{E}(x))e_2(x)(1 - H_{\epsilon}(\phi(x)))\right]dx \tag{8}$$

In this formulation, the amplitude parameter α bounds the maximum modulation. High-uncertainty neighborhoods (large $\hat{E}$) soften the commitment to either region, while low-uncertainty regions reinforce the appropriate side of the contour.

To preserve boundary smoothness and anatomical plausibility during evolution, a curvature-based regularization term is incorporated.

$$E_{\text{reg}}(\phi) = \int_{\Omega} |\nabla H_{\epsilon}(\phi(x))|dx = \int_{\Omega} \delta_{\epsilon}(\phi(x))|\nabla\phi(x)|dx \tag{9}$$

3.4. Variational Minimization and Gradient Descent

Minimization of the FEARE energy functional in (7) is performed via gradient descent with respect to the level-set function ϕ. Taking the variational (Euler-Lagrange) derivative yields the corresponding evolution equation.

$$\frac{\partial\phi}{\partial t} = \delta_{\epsilon}(\phi)\left[-(1 + \alpha\hat{E})e_1 + (1 - \alpha\hat{E})e_2\right] + \lambda\delta_{\epsilon}(\phi)\kappa(\phi) \tag{10}$$

In practical implementation, the continuous evolution equation (10) is discretized using an explicit time-marching scheme. The numerical update rule at iteration n is:

$$\phi^{n+1} = \phi^{n} + \Delta t\frac{\partial\phi}{\partial t}, \tag{11}$$

Where Δt is the time step. The level-set function is initialized as a signed-distance function and is periodically reinitialized to maintain numerical stability during evolution.

3.5. Practical Considerations and Interpretation

Curvature terms are computed using standard finite-difference schemes, while Gaussian convolutions and local histogram computations are implemented efficiently using separable filters. The bandwidth σ controls the locality of the statistics. The sigmoid slope γ determines the sensitivity to entropy variations and the amplitude α bounds the maximum modulation between region forces. The parameters λ and Δt balance data fidelity, smoothness, and numerical stability. Each iteration has linear computational complexity with respect to the number of pixels, and the implementation is readily parallelizable on CPU or GPU architectures.

From an intuitive standpoint, when the normalized entropy $\hat{E}(x)$ is small (low local uncertainty), the confidence modulation diminishes, and FEARE reduces to conventional localized region fitting. Conversely, in high-entropy regions characterized by weak boundaries or structural ambiguity, the entropy-driven modulation increases, thereby reducing the influence of potentially misleading local statistics and allowing the curvature regularization and neighboring confident regions to guide the contour evolution. This adaptive behavior enables robust segmentation in challenging pathological or low-contrast imaging scenarios where traditional region-based models often fail.

4. EXPERIMENTAL RESULTS AND DISCUSSION

4.1. Dataset, Annotation, and Evaluation Metrics

We apply the publicly available Sunnybrook Cardiac MRI dataset [12], which is an extensively used benchmark for medical image segmentation, to rigorously assess the proposed FEARE model. The dataset consists of short-axis cardiac MRI images from 45 patients, categorized into four pathological groups: normal (NOR), hypertrophy (HYP),

heart failure with infarction (HF-I), and heart failure without infarction (HF-NI). Expert-annotated ground truth delineations of the endocardial and epicardial boundaries are provided for both end-diastolic and end-systolic phases. Owing to the heterogeneity of cardiac morphology and pathology, this dataset is well-suited for evaluating segmentation robustness across diverse clinical conditions.

All experiments were performed in a two-dimensional, slice-by-slice manner, consistent with previous studies [10]. Ground truth annotations were used exclusively for quantitative evaluation. To ensure statistical reliability, a five-fold cross-validation protocol was adopted while preserving the pathological class distribution across folds. Segmentation performance was evaluated using an extensive set of metrics, including overlap-based measures (Dice Similarity Coefficient, Intersection over Union, Precision, and Recall), boundary-based measures (Average Perpendicular Distance, Mean Absolute Distance, Hausdorff Distance, and Fractal Dimension), and computational efficiency indicators (execution time and memory usage). This combination captures not only spatial accuracy but also boundary fidelity and computational practicality, which are essential for clinical applicability.

Comparative evaluation was performed against nine representative active contour models selected based on their methodological relevance to the proposed approach. These include classical region-based formulations such as Chan and Vese [4], Local Binary Fitting (LBF) [6], and Local Gaussian Distribution Fitting (LGDF) [26], as well as more recent fuzzy and hybrid energy-based models that incorporate adaptive region terms or pressure-force mechanisms [7, 9, 13]. All baseline methods were independently reimplemented in MATLAB or adapted from publicly available implementations and executed on the same input cardiac MRI images as the proposed FEARE model. Identical preprocessing, initialization strategies, evaluation metrics, and cross-validation folds were used for all methods, ensuring that the reported performance values were obtained under uniform experimental conditions rather than adopted from external sources. For each method, parameter selection was guided by validation performance within the respective cross-validation folds, following commonly adopted evaluation practices in the literature.

As part of the experimental setup, all cardiac MRI images were processed using a standardized preprocessing pipeline to ensure reproducibility and stability across subjects and pathological conditions. Images were resampled to a uniform in-plane resolution of 256×256 pixels to mitigate acquisition-dependent scale variations. Slice-wise linear intensity normalization was applied to map pixel values into the $[0, 1]$ range, and intensity values outside the 1st–99th percentile were clipped to suppress extreme outliers. No explicit denoising filters were employed; instead, robustness to noise was achieved implicitly through the entropy-adaptive region energy formulation of the proposed model.

4.2. FEARE Pathology-Wise Performance

The proposed FEARE model demonstrated consistent and robust segmentation performance across four cardiac pathologies in the Sunnybrook Cardiac MRI dataset [12] as summarized in Table 1. The Dice Similarity Coefficient (DSC) remained above 0.75 across all categories, peaking at 0.8704 in HF-I, indicating accurate delineation in infarcted myocardial regions. HF-NI recorded the lowest standard deviation (0.0427), indicating excellent intra-class consistency. Notably, all classes achieved maximum DSC values exceeding 0.96, underscoring FEARE's precision in capturing anatomical boundaries. Meanwhile, Intersection over Union (IoU) ranged from 0.6497 (HYP) to 0.7978 (HF-I), reaffirming the model's generalizability to heterogeneous pathologies and imaging conditions. These results confirm FEARE's potential for clinical-grade segmentation by balancing statistical consistency, anatomical accuracy, and robustness to pathology-specific variations.

Table 1. Pathology-wise segmentation performance of FEARE on the Sunnybrook dataset using Dice Similarity Coefficient (DSC) and Intersection over Union (IoU).

Pathology	Mean DSC	Median DSC	Std. Dev (DSC)	Min DSC	Max DSC	Mean IoU
Healthy	0.8629	0.9323	0.1211	0.5955	0.9699	0.7761
HF-I	0.8704	0.9265	0.1633	0.4145	0.9728	0.7978
HF-NI	0.8680	0.8683	0.0427	0.7328	0.9194	0.7690
HYP	0.7468	0.8860	0.2622	0.1444	0.9527	0.6497

4.3. Comparative Evaluation

As summarized in Table 2, the proposed FEARE model achieved the highest Mean DSC (0.8456) and Mean IoU (0.7572) among all tested segmentation methods, while also registering the fewest total failures (6). In contrast, conventional models such as LBF and LGDF, despite their competitive overlap accuracies, exhibited moderately higher failure rates. Methods like WHRSPF and FRAGL demonstrated considerable segmentation instability, as indicated by their substantially lower IoU scores and elevated failure frequencies. These findings underscore FEARE's ability to achieve robust segmentation accuracy with minimal errors, even across diverse cardiac pathologies.

Table 2. Quantitative comparison of segmentation methods on cardiac MRI images across all pathologies using various performance metrics.

Method	Mean DSC	Median DSC	Std DSC	Min DSC	Max DSC	Mean IoU	Failures
LBF [6]	0.7905	0.8718	0.2176	0.0000	0.9719	0.6940	23
LGDF [26]	0.6034	0.6423	0.2293	0.1189	0.9697	0.4698	35
LIF [14]	0.7475	0.8557	0.2385	0.1257	0.9668	0.6451	16
LPF [3]	0.5883	0.6233	0.2082	0.1261	0.9232	0.4468	37
WHRSPF [13]	0.3374	0.0000	0.3860	0.0000	0.9406	0.2793	44
FRAGL [7]	0.5994	0.7430	0.3610	0.0000	0.9641	0.5178	22
GLFIF [8]	0.6810	0.6889	0.2494	0.0685	0.9729	0.5680	31
HLFRA [9]	0.6561	0.8317	0.3494	0.0000	0.9679	0.5740	22
ERAC [27]	0.6553	0.8285	0.3401	0.0000	0.9768	0.5699	25
FEARE-Proposed	0.8456	0.9021	0.1568	0.1444	0.9728	0.7572	6

Note: DSC – Dice Similarity Coefficient; IoU – Intersection over Union.

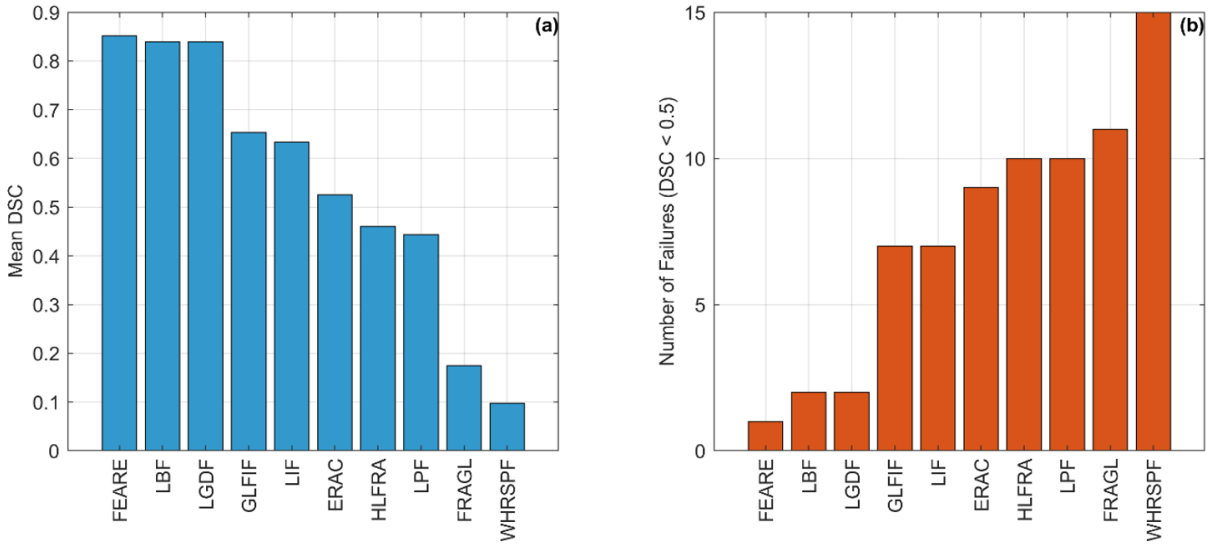

Figure 1. Comparative analysis of segmentation performance across methods for a single-patient case from the Healthy pathology subset — (a) Mean DSC, (b) Number of failures (DSC < 0.5).

Furthermore, a detailed analysis using a representative case from the Healthy pathology subset, as shown in Figure 1, highlights the superior performance of the FEARE model. It recorded the highest Mean DSC (0.8516) and Mean IoU (0.7681), with only a single failure case (DSC < 0.5). In contrast, methods like WHRSPF and FRAGL

showed significantly reduced segmentation reliability, with 15 and 11 failure cases respectively. These results further validate FEARE's high segmentation fidelity, generalizability, and consistent performance across both normal and pathological cardiac MRI structures.

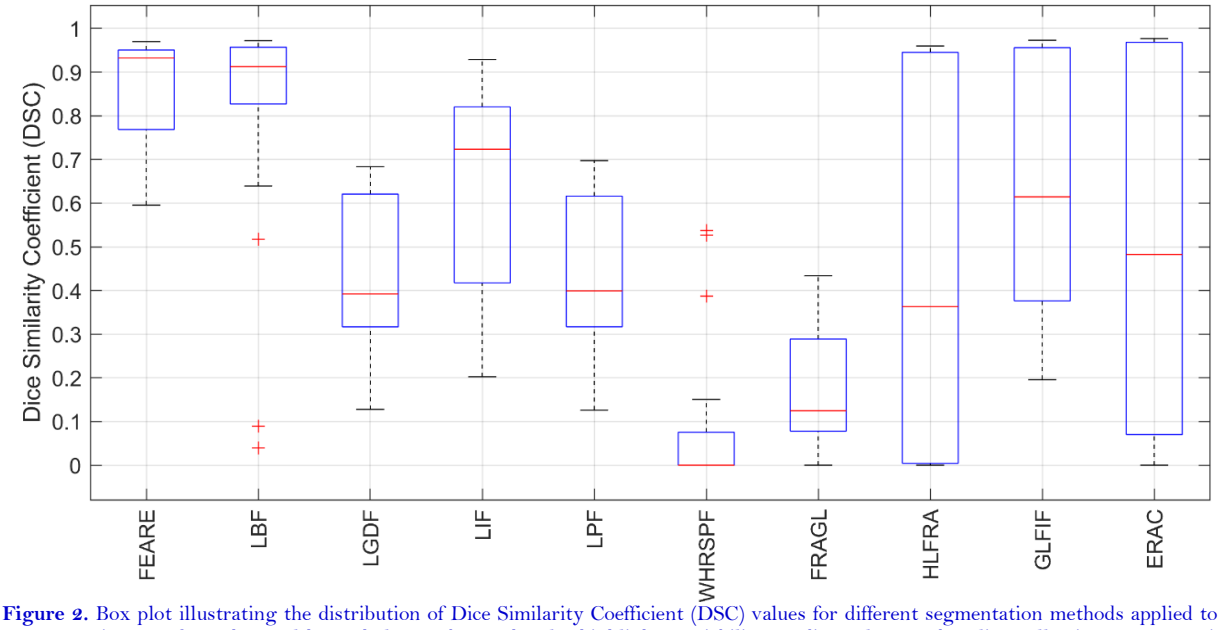

Figure 2. Box plot illustrating the distribution of Dice Similarity Coefficient (DSC) values for different segmentation methods applied to a representative case from the Healthy pathology subset. The plot highlights variability, median values, and outliers, allowing a comparative assessment of segmentation robustness across methods.

4.4. Statistical Robustness and Failure Analysis

The box plot in Figure 2 illustrates the segmentation performance variation across methods for a representative patient from the Healthy pathology subset. The FEARE model demonstrates the highest median Dice Similarity Coefficient (DSC) and the narrowest interquartile range (IQR), indicating excellent stability and minimal variability across segmentations. In contrast, methods such as FRAGL, HLFRA, and WHRSPF exhibit broader spreads with numerous outliers, highlighting inconsistent segmentation performance, even under normal anatomical conditions. Although traditional models like LBF and LGDF achieve relatively high median DSC values, their wider IQRs suggest increased sensitivity to case-specific anatomical variability. Hence, Figure 2 clearly reinforces that FEARE not only achieves superior segmentation accuracy but also delivers robust, pathology-invariant performance.

4.5. Summary of Insights

The experimental evaluation across pathology-specific, comparative, and statistically robust analyses collectively substantiates the superior performance of the proposed FEARE model. It consistently achieved the highest Dice Similarity Coefficient (DSC) and Intersection over Union (IoU) scores, while maintaining the lowest failure rates across both population-wide and single-case evaluations. Notably, FEARE exhibited remarkable resilience to anatomical variability and noise, as evidenced by its narrow interquartile range and minimal outliers in box plots. These findings demonstrate that FEARE not only delivers accurate segmentation but also ensures statistical reliability and generalization across diverse cardiac pathologies, outperforming conventional and contemporary models in both stability and precision.

4.6. Metric-wise Comparative Analysis

Figures 3–6 and Table 3 present a comprehensive, pathology-specific evaluation of ten segmentation methods across four cardiac conditions: Healthy, Heart Failure with Infarction (HF-I), Heart Failure without Infarction (HF-NI), and Left Ventricular Hypertrophy (HYP).

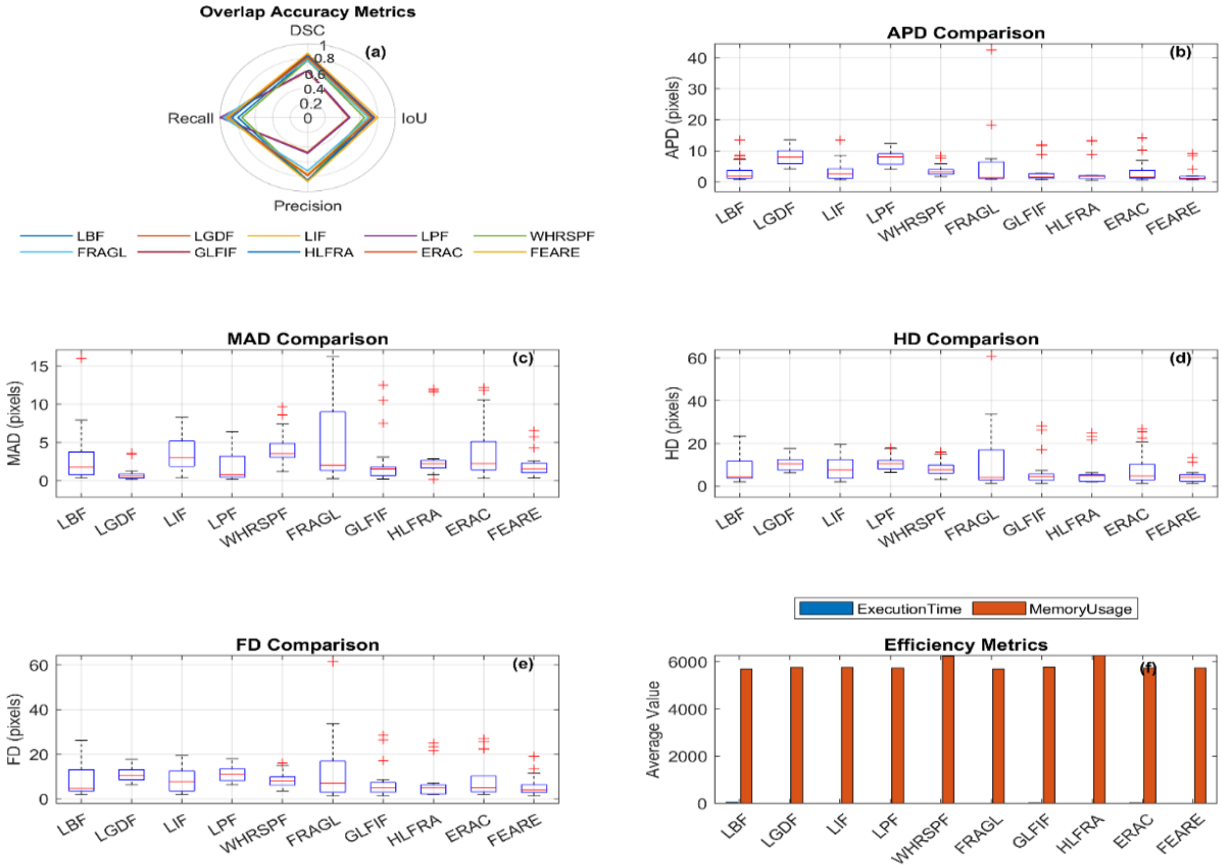

Figure 3. Composite evaluation of segmentation methods on Healthy cardiac MRI data: (a) Overlap accuracy metrics (radar plot: DSC, IoU, Precision, Recall); (b) Average Perpendicular Distance (APD); (c) Mean Absolute Deviation (MAD); (d) Hausdorff Distance (HD); (e) Fourier Distance (FD); (f) Efficiency (execution time and memory usage). Higher is better for DSC/IoU/Precision/Recall; lower is better for APD/MAD/HD/FD.

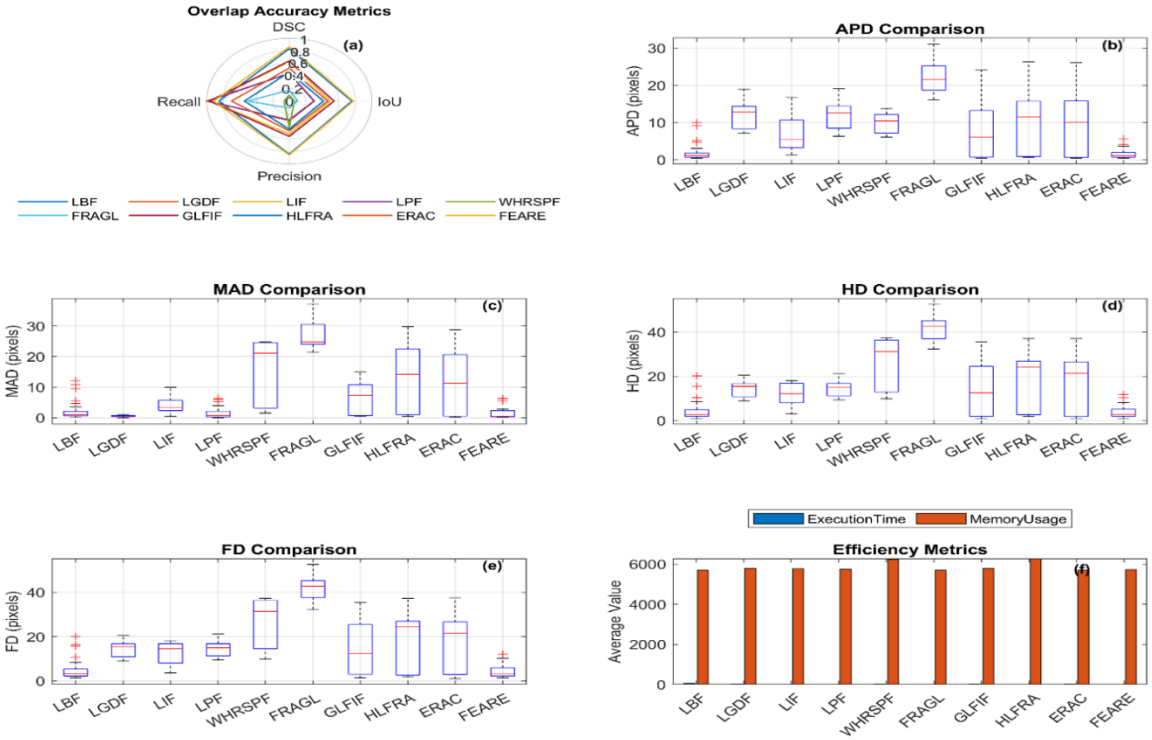

Figure 4. Composite evaluation of segmentation methods on Heart Failure with Infarction (HF-I) cardiac MRI data: (a) Overlap accuracy metrics (radar plot: DSC, IoU, Precision, Recall); (b) Average Perpendicular Distance (APD); (c) Mean Absolute Deviation (MAD); (d) Hausdorff Distance (HD); (e) Fourier Distance (FD); (f) Efficiency (execution time and memory usage). Higher is better for DSC/IoU/Precision/Recall; lower is better for APD/MAD/HD/FD.

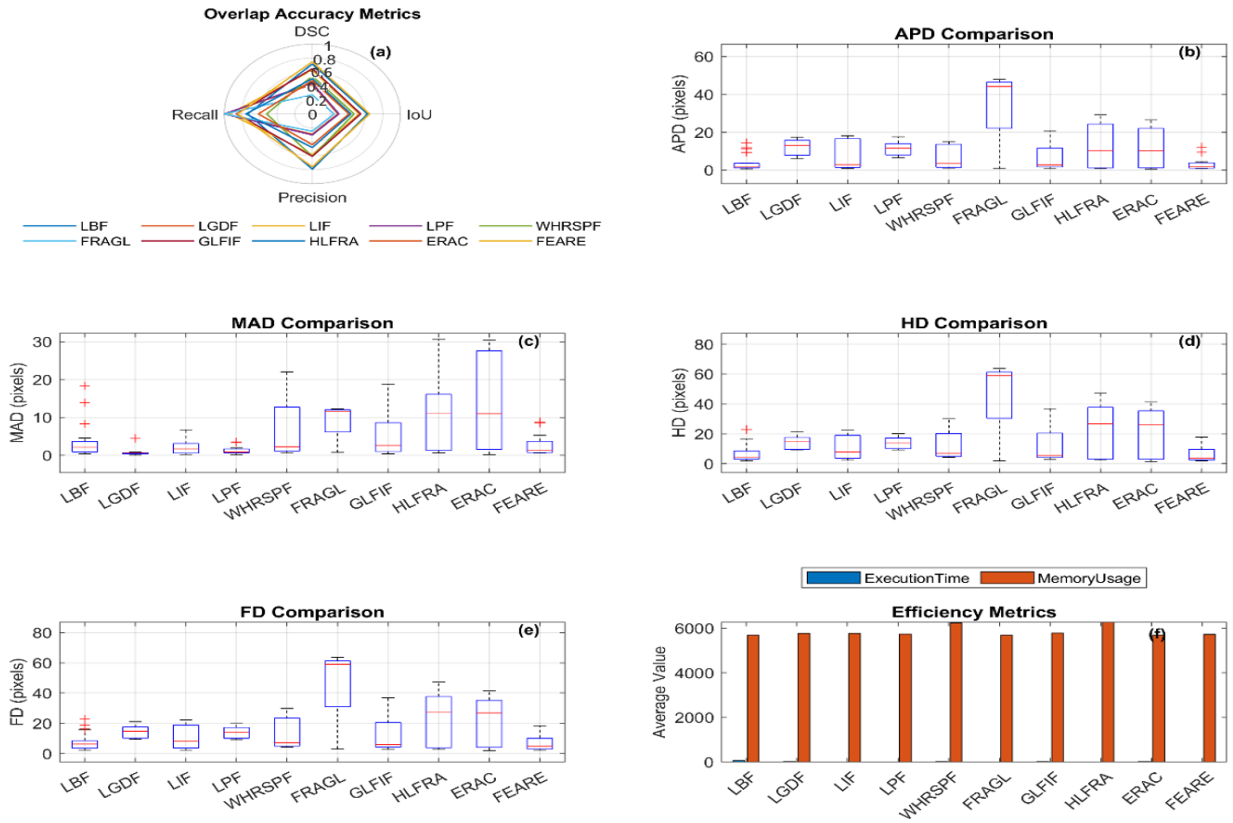

Figure 5. Composite evaluation of segmentation methods on Heart Failure without Infarction (HF-NI) cardiac MRI data: (a) Overlap accuracy metrics (radar plot: DSC, IoU, Precision, Recall); (b) APD; (c) MAD; (d) HD; (e) FD; (f) Efficiency (execution time and memory usage). Higher is better for DSC/IoU/Precision/Recall; lower is better for APD/MAD/HD/FD.

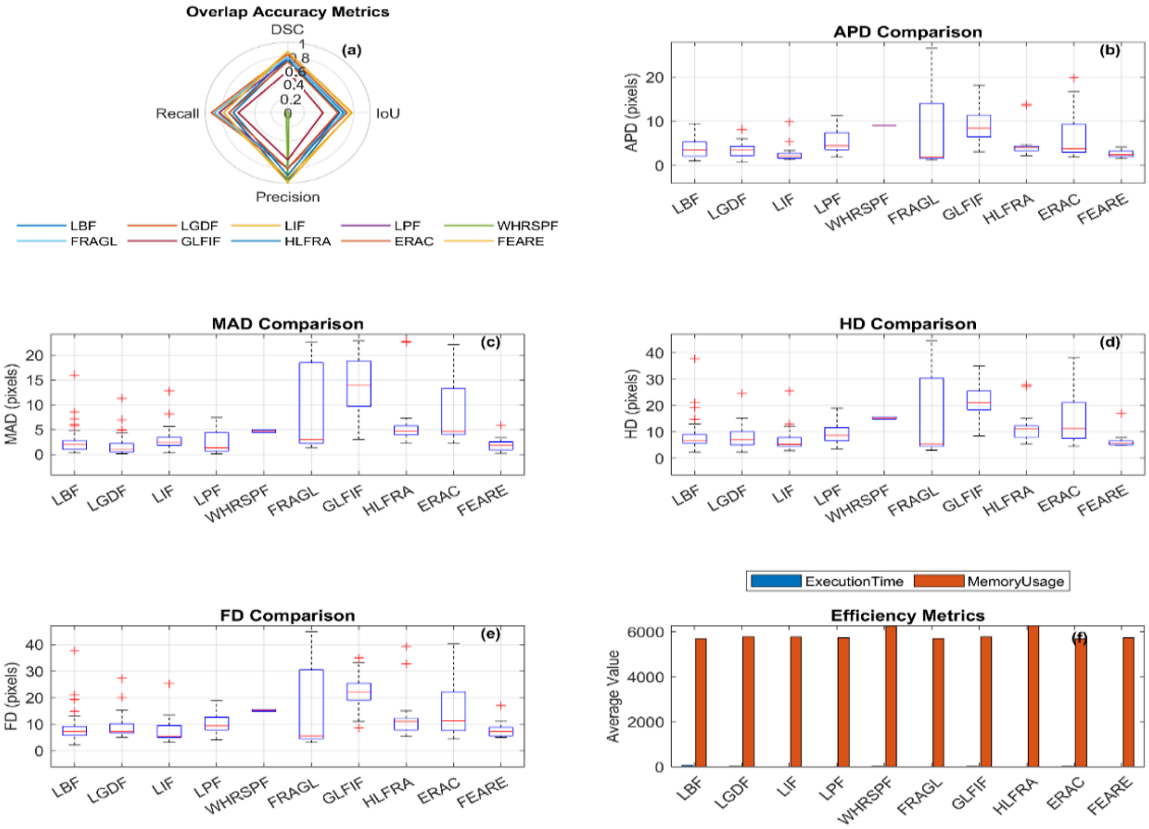

Figure 6. Composite evaluation of segmentation methods on Left Ventricular Hypertrophy (HYP) cardiac MRI data: (a) Overlap accuracy metrics (radar plot: DSC, IoU, Precision, Recall); (b) APD; (c) MAD; (d) HD; (e) FD; (f) Efficiency (execution time and memory usage). Higher is better for DSC/IoU/Precision/Recall; lower is better for APD/MAD/HD/FD.

The analysis encompasses three major dimensions: overlap accuracy, boundary error, and computational efficiency. Across all pathologies, the FEARE model consistently demonstrates superior performance in overlap-based metrics, as evidenced by the radar plots in subfigures (a) in Figures 3–6. Notably, FEARE achieves the highest Dice Similarity Coefficient (DSC), Intersection over Union (IoU), Precision, and Recall across the board. These observations are further substantiated by the average metric values in the upper portion of Table 3, where FEARE achieves a DSC of 0.85 and a Recall of 0.86, surpassing all other models, including LBF, LGDF, and WHRSPF. Subfigures (b) through (e) in Figures 3–6 depict the boundary error distributions across metrics such as Average Perpendicular Distance (APD), Mean Absolute Deviation (MAD), Hausdorff Distance (HD), and Fourier Distance (FD). The FEARE model consistently exhibits narrower interquartile ranges, lower median errors, and fewer outliers, signifying enhanced robustness and anatomical boundary adherence even under pathological variations. In contrast, methods such as WHRSPF and FRAGL display wider variability and reduced boundary fidelity, particularly in infarcted or hypertrophic cases.

Efficiency metrics, shown in subfigure (f) of each figure and summarized in the lower section of Table 3, further underscore FEARE's practical suitability. Despite delivering the highest segmentation accuracy, FEARE maintains a competitive execution time of 0.26 seconds and a modest memory usage of 5735.66 MB. This balance makes it viable for real-time inference or resource-constrained deployment. By comparison, legacy models like LBF incur significant computational overhead, with execution times exceeding 62 seconds. Collectively, this metric-wise comparative analysis underscores FEARE's strong generalization capability, boundary precision, and computational efficiency, establishing its readiness for clinical translation across a broad spectrum of cardiac pathologies.

Table 3. Quantitative evaluation of overlap-based region metrics (DSC, IoU, Precision, Recall) and boundary error metrics (APD, MAD, HD, FD), along with efficiency measures (Execution time and memory usage), averaged across multiple cardiac pathologies. FEARE achieves the best trade-off between segmentation accuracy, robustness, and computational efficiency compared to competing models.

Method/ Metrics	DSC	IoU	Precision	Recall	APD
LBF [6]	0.79	0.69	0.88	0.77	3.08
LGDF [26]	0.60	0.47	0.49	0.98	8.53
LIF [14]	0.75	0.65	0.72	0.91	4.79
LPF [3]	0.59	0.45	0.50	0.94	8.75
WHRSPF [13]	0.34	0.28	0.67	0.31	6.41
FRAGL [7]	0.60	0.52	0.56	0.83	12.72
GLFIF [8]	0.68	0.57	0.68	0.82	6.73
HLFRA [9]	0.66	0.57	0.69	0.70	6.86
ERAC [27]	0.66	0.57	0.65	0.75	7.46
FEARE-Proposed	0.85	0.76	0.88	0.86	2.41
Method/ Metrics	MAD	HD	FD	Execution Time	Memory Usage
LBF [6]	2.73	7.05	7.49	62.83	5698.82
LGDF [26]	1.14	11.48	12.02	0.14	5777.50
LIF [14]	3.36	9.47	9.77	0.76	5766.43
LPF [3]	1.85	11.87	12.25	0.69	5738.89
WHRSPF [13]	8.13	14.73	15.13	0.13	6243.69
FRAGL [7]	11.91	23.17	23.45	0.25	5702.52
GLFIF [8]	7.43	14.27	14.66	0.06	5780.14
HLFRA [9]	8.13	13.78	14.19	0.56	6275.94
ERAC [27]	8.90	14.84	15.41	0.09	5710.64
FEARE-Proposed	2.03	5.44	6.21	0.26	5735.66

5. ABLATION STUDY ON ENTROPY WEIGHTING AND SIGMOID SCALING PARAMETERS

To further validate the robustness and sensitivity of the proposed FEARE model, we conducted a comprehensive ablation study by systematically varying two key parameters: the entropy weighting factor α and the sigmoid scaling parameter γ. These parameters critically influence the shape-fitting behavior and boundary localization of the active contour. The experiment was performed across multiple combinations of $\alpha \in (0.4,0.6)$ and $\gamma \in (8,9,10)$, and the resulting segmentations were evaluated using standard metrics, including DSC, IoU, Precision, Recall, and APD.

Table 4 summarizes quantitative results for two representative cases (Image 3 and Image 5) drawn from the cardiac MRI dataset. For Image 3, increasing γ from 8 to 10 while keeping $\alpha = 0.4$ improves DSC from 0.9196 to 0.9234, indicating better contour convergence. IoU and Precision follow the same trend, whereas a higher α (0.6) produces a slight decrease in Recall, while APD remains essentially unchanged. These observations suggest that a moderate entropy weight amplitude maintains boundary sharpness without over-suppressing fine edges.

For Image 5, DSC is comparatively stable across all (γ, α) combinations, with a small decline in Recall as α increases; IoU, Precision, and APD vary only marginally. This indicates that, for this anatomy, FEARE is relatively insensitive to the tested parameter ranges, while a lower α helps avoid recall loss. Overall, the configuration $(\gamma = 9, \alpha = 0.4)$ provides the best balance among DSC, IoU, Precision, Recall, and APD, and is therefore adopted as the default setting in subsequent experiments.

Table 4. Quantitative impact of varying entropy weight (α) and sigmoid slope (γ) on segmentation accuracy for two representative cardiac images. Reported metrics include Dice Similarity Coefficient (DSC), Intersection over Union (IoU), Precision, Recall, and Average Perpendicular Distance (APD). Results highlight FEARE's robustness to parameter variations.

Image No.	γ	α	DSC	IoU	Precision	Recall	APD
3	8	0.4	0.9196	0.8528	0.9181	0.9258	1.2553
	8	0.6	0.9202	0.8547	0.9254	0.9193	1.2266
	9	0.4	0.9211	0.8553	0.9217	0.9248	1.2347
	9	0.6	0.9213	0.8556	0.9257	0.9215	1.2247
	10	0.4	0.9232	0.8592	0.9317	0.9197	1.2216
	10	0.6	0.9223	0.8580	0.9308	0.9187	1.2255
5	8	0.4	0.9065	0.8326	0.9733	0.8550	1.4653
	8	0.6	0.9065	0.8326	0.9733	0.8550	1.4653
	9	0.4	0.9100	0.8386	0.9712	0.8621	1.4104
	9	0.6	0.9100	0.8386	0.9712	0.8621	1.4104
	10	0.4	0.9065	0.8322	0.9680	0.8592	1.4833
	10	0.6	0.9065	0.8322	0.9680	0.8592	1.4833

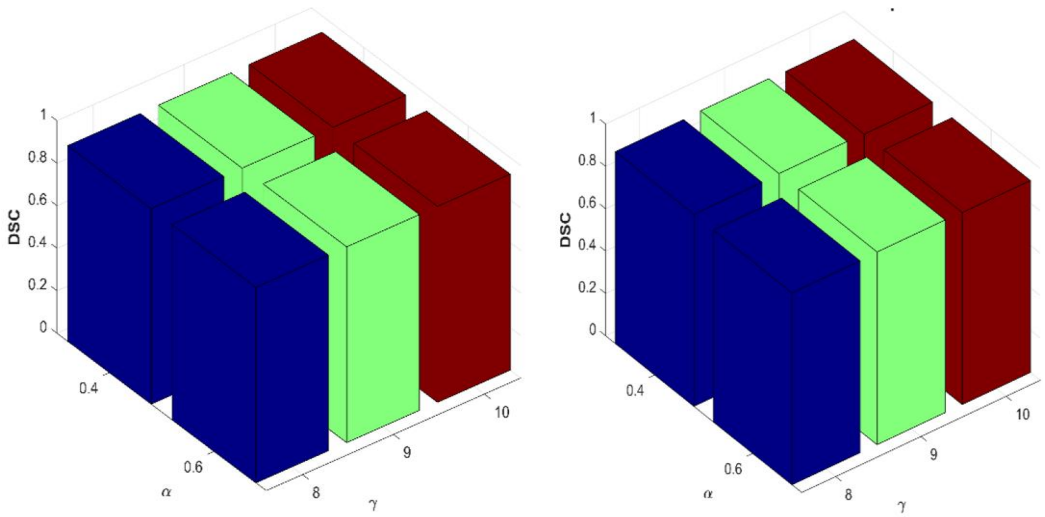

Figure 7. Three-dimensional plots showing DSC variation with entropy weight (α) and sigmoid slope (γ) for two representative images. The consistently high DSC across the evaluated parameter space confirms FEARE's robust entropy-driven fitting mechanism and stable performance under parameter changes.

Image 5 (right half of Table 4) shows a slightly different trend: DSC remains essentially stable across all (γ, α) settings, while Recall exhibits a mild decrease as α increases; IoU, Precision, and APD change only marginally. This indicates that, for this anatomy, FEARE is largely insensitive to the tested parameter ranges and that using a lower α mitigates recall loss. Accordingly, we adopt $(\gamma = 9, \alpha = 0.4)$ as the default configuration, as it offers the best overall balance among DSC, IoU, Precision, Recall, and APD.

To visually interpret the trends, Figure 7 plots the 3D bar graphs of DSC values for each α–γ combination for the same two images. The plots reveal that γ = 9 with α = 0.4 provides consistently high DSC across both images, thus suggesting an optimal trade-off between entropy regularization and sigmoid-driven fitting force modulation. Overall, this ablation confirms that FEARE maintains high segmentation fidelity across a reasonable range of α and γ. The combination (γ = 9, α = 0.4) achieves the best balance between region homogeneity and edge precision, and is thus selected as the default configuration for all subsequent experiments.

6. QUALITATIVE COMPARISON OF SEGMENTATION RESULTS

To ensure visual clarity and interpretability, we present qualitative comparisons using three representative baseline methods, LBF, LIF, and LGDF, together with the proposed FEARE model. These methods were selected due to their foundational roles in active contour-based segmentation and their distinct strategies for contour evolution. Including all nine baselines would result in visual redundancy and overcrowded figures; hence, the most informative representatives were chosen. Figures 8–11 illustrate segmentation overlays on representative cardiac images from four distinct pathological categories: Heart Failure with Infarction (HF-I), Heart Failure without Infarction (HF-NI), Left Ventricular Hypertrophy (HYP), and Healthy subjects. In each figure, subplots (a)–(d) correspond to LBF, LIF, LGDF, and the proposed FEARE method, respectively. Green contours indicate the ground truth, while red contours denote model predictions.

Across all categories, FEARE demonstrates superior alignment with ground truth, capturing anatomical boundaries more accurately, even under challenging conditions such as shape irregularity, low contrast, or noise. In contrast, LBF and LIF often deviate in boundary adherence, especially in infarcted or hypertrophied regions, while LGDF produces smoother results but fails to preserve finer ventricular details. These visual results corroborate the earlier quantitative metrics, affirming the robustness and precision of FEARE across both pathological and normal cardiac image scenarios.

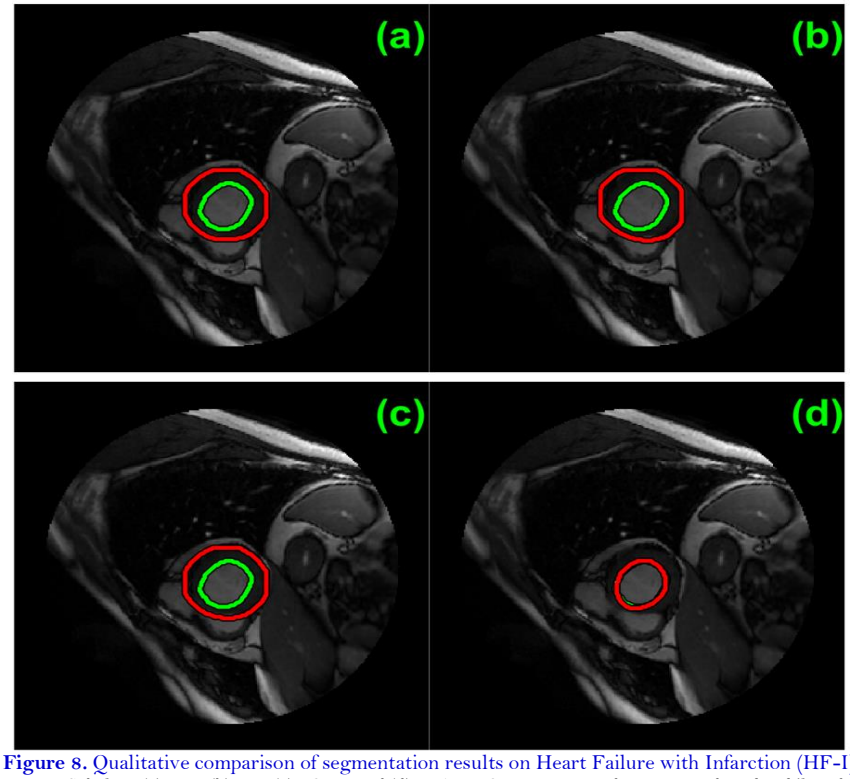

Figure 8. Qualitative comparison of segmentation results on Heart Failure with Infarction (HF-I).
Note: Subplots: (a) LBF, (b) LIF, (c) LGDF, and (d) FEARE. Green contours denote ground truth, while red contours represent predicted boundaries.

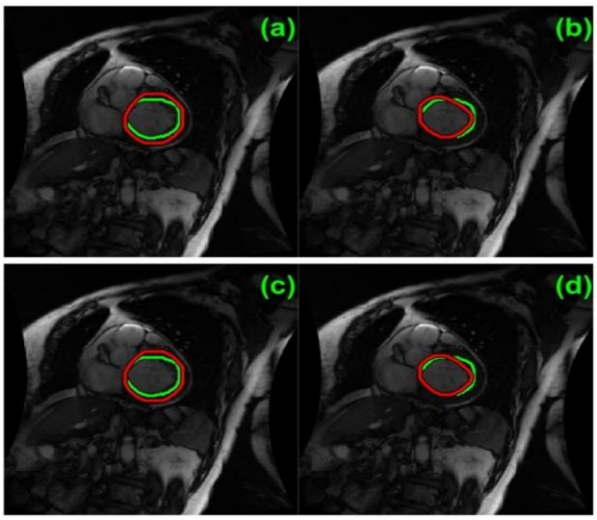

Figure 9. Qualitative comparison of segmentation results on Heart Failure without Infarction (HF-NI).

Note: Subplots: (a) LBF, (b) LIF, (c) LGDF, and (d) FEARE. Green contours denote ground truth, while red contours represent predicted boundaries.

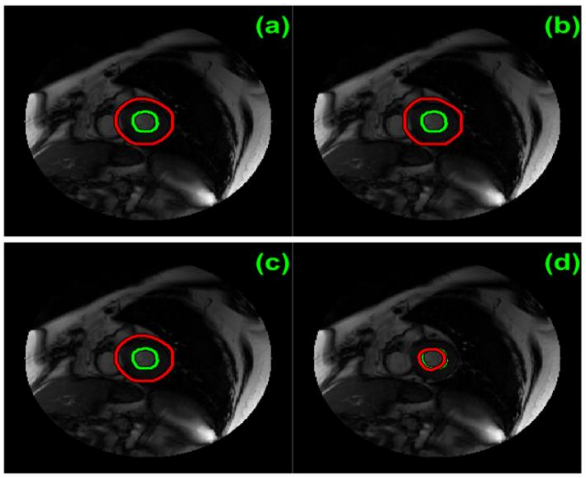

Figure 10. Qualitative comparison of segmentation results on Left Ventricular Hypertrophy (HYP).

Note: Subplots: (a) LBF, (b) LIF, (c) LGDF, and (d) FEARE. Green contours denote ground truth, while red contours represent predicted boundaries.

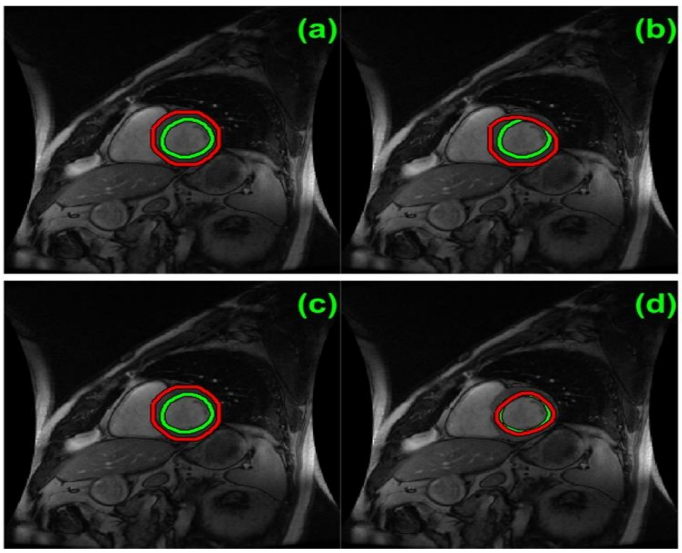

Figure 11. Qualitative comparison of segmentation results on Healthy subjects.

Note: Subplots: (a) LBF, (b) LIF, (c) LGDF, and (d) FEARE. Green contours denote ground truth, while red contours represent predicted boundaries.

7. DISCUSSION AND LIMITATIONS

Across the evaluated cardiac pathology groups, FEARE demonstrates an overall performance gain supported by statistical analysis. Results from the paired Wilcoxon signed-rank test on per-case Dice similarity coefficient values (Table 5) indicate that FEARE achieves significantly higher accuracy than the recent ERAC method for each pathology category considered. Beyond improvements in mean accuracy, the analysis further shows that FEARE produces more stable segmentation outcomes on a case-by-case basis, particularly in scenarios characterized by heterogeneous or visually challenging image conditions.

Table 5. Paired statistical significance testing of FEARE versus the recent ERAC method using per-case Dice similarity coefficient (DSC) values.

Pathology	N	Median ΔDSC	Mean ΔDSC	P-value
Healthy	17	0.310	0.337	0.008
HF-I	18	0.021	0.054	0.002
HF-NI	20	0.046	0.141	0.000
HYP	12	0.158	0.268	0.008

However, it is important to note some limitations. One such limitation is the dependence on parameters. As a result, FEARE currently relies on a small number of parameters, including the entropy slope, entropy weighting factor, and local kernel bandwidth, which were selected according to a systematic but manual test. Although this process enhances the interpretability and numerical reliability of the model, it can also restrict the scalability across datasets of different properties. Consequently, we propose to investigate adaptive parameter selection approaches, such as bilevel optimization or Bayesian optimization, that may alleviate unnecessary manual intervention and enhance generalization. In the meantime, infusing FEARE with edge-aware contour mechanisms and data-efficient semi-supervised learning frameworks could be a means of enhancing adaptability, but at the same time, preserving the transparency of the model.

A further consideration concerns computational efficiency. Although FEARE remains substantially lighter than fully learning-based segmentation frameworks, the inclusion of geometry-aware regularization and shape-conformity constraints inevitably increases computational load, particularly for high-resolution images and volumetric data. This is reflected in the runtime evaluation, where FEARE does not emerge as the fastest among the compared methods; certain local fitting approaches benefit from simpler energy formulations and therefore achieve shorter execution times. Even so, FEARE remains practically viable and avoids the extensive training and inference costs associated with region-scalable or hybrid deep learning models. Additional optimizations, including GPU acceleration, narrow-band evolution strategies, and optimized convolution–histogram implementations, are expected to further mitigate runtime overhead.

The scope of experimental validation also warrants discussion. Currently, evaluation is limited to cardiac magnetic resonance imaging. Although the underlying formulation is not modality-specific, direct validation on other imaging modalities, such as computed tomography, ultrasound, and positron emission tomography, has yet to be performed and remains an important direction for future research. Isolated failure cases were observed under conditions of extremely low contrast or pronounced anatomical occlusion, where entropy-based cues alone proved insufficient for accurate boundary delineation. In such cases, incorporating complementary edge-based information or statistical and learned shape priors is likely to enhance robustness.

FEARE can provide a transparent and data-efficient alternative to purely learning-driven segmentation approaches. Although modern deep neural networks can attain high accuracy given access to large volumes of annotated data, interpretability is often low and the computational resources required are usually very expensive. FEARE complements these methods by providing a training-free and analytically grounded framework with statistically validated performance advantages. The future incorporation of lightweight learned priors within the entropy-driven formulation is expected to further improve robustness, automation, and clinical applicability.

8. CONCLUSION

In this paper, we presented FEARE (Fuzzy Entropy Adaptive Region Energy), which is an innovative energy-based segmentation scheme developed to tackle the major barriers in segmentation through medical images (e.g., complex textures, boundary ambiguity, region-specific structural variability).

FEARE dynamically adjusts to spatial uncertainty in a way that retains contour regularity by employing a dedicated shape conformity term, and combining fuzzy entropy-guided confidence modulation and adaptive region fitting. A large-scale implementation of FEARE on clinical, real-life cardiac MRI with multiple pathological states revealed a consistent performance boost over nine well-known active contour models on many quantitative metrics. It demonstrated better segmentation performance, boundary behavior, and robustness to noise and irregular shapes. Although the present framework was tested with cardiac MRI for initial evaluation, the proposed design approach with locally adaptable, uncertainty-weighted, and geometry-aware regularization gives significant credence to FEARE as a generalizable and flexible tool for segmentation, which is applicable to other applications in medical imaging as well as to much broader computer vision applications.

FEARE will also be expanded to multimodal datasets and learning-based priors for improved automation and performance. Meanwhile, TVC advancements on edge-aware ACMs [17] and semi-supervised nnU-Net variants [25] indicate that hybridization with FEARE can complement each other. From a clinical and engineering perspective, FEARE represents a straightforward data-efficient alternative for segmentation, achieving reliable execution free from the requirement of large annotated data sets, fine-tuning of parameters, or non-trivial decision-making processes that are hallmarks of deep learning models.

Funding: The authors received no financial support for the research, authorship, and/or publication of this article. No external grant was received for this study.
Institutional Review Board Statement: Not applicable.
Transparency: The authors state that the manuscript is honest, truthful, and transparent, that no key aspects of the investigation have been omitted, and that any differences from the study as planned have been clarified. This study followed all writing ethics.
Competing Interests: The authors declare that they have no competing interests.
Authors' Contributions: Both authors contributed equally to the conception and design of the study. Both authors have read and agreed to the published version of the manuscript.

REFERENCES

[1] G. Litjens *et al.*, "A survey on deep learning in medical image analysis," *Medical Image Analysis*, vol. 42, pp. 60-88, 2017. https://doi.org/10.1016/j.media.2017.07.005

[2] K. Ding, L. Xiao, and G. Weng, "Active contours driven by region-scalable fitting and optimized Laplacian of Gaussian energy for image segmentation," *Signal Processing*, vol. 134, pp. 224-233, 2017. https://doi.org/10.1016/j.sigpro.2016.12.021

[3] K. Ding, L. Xiao, and G. Weng, "Active contours driven by local pre-fitting energy for fast image segmentation," *Pattern Recognition Letters*, vol. 104, pp. 29-36, 2018. https://doi.org/10.1016/j.patrec.2018.01.019

[4] T. F. Chan and L. A. Vese, "Active contours without edges," *IEEE Transactions on Image Processing*, vol. 10, no. 2, pp. 266-277, 2001. https://doi.org/10.1109/83.902291

[5] M. Kass, A. Witkin, and D. Terzopoulos, "Snakes: Active contour models," *International Journal of Computer Vision*, vol. 1, no. 4, pp. 321-331, 1988. https://doi.org/10.1007/BF00133570

[6] C. Li, C.-Y. Kao, J. C. Gore, and Z. Ding, "Implicit active contours driven by local binary fitting energy," in *Proceedings of the IEEE Conference on Computer Vision and Pattern Recognition (CVPR)*, 2007, pp. 1–7.

[7] J. Fang, H. Liu, L. Zhang, J. Liu, and H. Liu, "Active contour driven by weighted hybrid signed pressure force for image segmentation," *IEEE Access*, vol. 7, pp. 97492-97504, 2019. https://doi.org/10.1109/ACCESS.2019.2929659

[8] J. Fang, H. Liu, J. Liu, H. Zhou, L. Zhang, and H. Liu, "Fuzzy region-based active contour driven by global and local fitting energy for image segmentation," *Applied Soft Computing*, vol. 100, p. 106982, 2021. https://doi.org/10.1016/j.asoc.2020.106982

[9] J. Fang, H. Liu, L. Zhang, J. Liu, and H. Liu, "Region-edge-based active contours driven by hybrid and local fuzzy region-based energy for image segmentation," *Information Sciences*, vol. 546, pp. 397-419, 2021. https://doi.org/10.1016/j.ins.2020.08.078

[10] H. Lv, F. Zhang, and R. Wang, "Robust active contour model using patch-based signed pressure force and optimized fractional-order edge," *IEEE Access*, vol. 9, pp. 8771-8785, 2021. https://doi.org/10.1109/ACCESS.2021.3049513

[11] D. Ma, Q. Liao, Z. Chen, R. Liao, and H. Ma, "Adaptive local-fitting-based active contour model for medical image segmentation," *Signal Processing: Image Communication*, vol. 76, pp. 201-213, 2019. https://doi.org/10.1016/j.image.2019.05.006

[12] Cardiac Atlas Project, "Cardiac Atlas Project: Sunnybrook cardiac MRI dataset (Sunnybrook Cardiac Data)," Retrieved: https://www.cardiacatlas.org/sunnybrook-cardiac-data/. [Accessed 19 Dec 2025], 2025.

[13] X. Meng and S. Si, "Active contour model based on hybrid signed pressure force function," *IET Image Processing*, vol. 17, no. 13, pp. 3702-3712, 2023. https://doi.org/10.1049/ipr2.12891

[14] K. Zhang, H. Song, and L. Zhang, "Active contours driven by local image fitting energy," *Pattern Recognition*, vol. 43, no. 4, pp. 1199-1206, 2010. https://doi.org/10.1016/j.patcog.2009.10.010

[15] X. Bai and G. Sapiro, "Geodesic active contours on implicit surfaces," *IEEE Transactions on Pattern Analysis and Machine Intelligence*, vol. 26, no. 3, pp. 324–337, 2004.

[16] N. Paragios and R. Deriche, "Geodesic active regions and level set methods for supervised texture segmentation," *International Journal of Computer Vision*, vol. 46, no. 3, pp. 223-247, 2002. https://doi.org/10.1023/A:1014080923068

[17] F. Zhang, X. Bi, G. Wang, G. Weng, and Y. Chen, "Anisotropic edge-enhanced active contour model with Gaussian difference for robust multi-category image segmentation," *The Visual Computer*, vol. 41, no. 12, pp. 10153-10170, 2025. https://doi.org/10.1007/s00371-025-04026-0

[18] O. Ronneberger, P. Fischer, and T. Brox, "U-Net: Convolutional networks for biomedical image segmentation," presented at the International Conference on Medical image Computing and Computer-Assisted Intervention, Springer, 2015.

[19] Z. Cheng, A. Qu, and X. He, "Contour-aware semantic segmentation network with spatial attention mechanism for medical image," *The Visual Computer*, vol. 38, no. 3, pp. 749-762, 2022. https://doi.org/10.1007/s00371-021-02075-9

[20] Q. Chen, Z. Xu, and X. Fang, "CaVMamba: Convolution-augmented VMamba for medical image segmentation," *The Visual Computer*, vol. 41, no. 8, pp. 5855-5872, 2025. https://doi.org/10.1007/s00371-024-03756-x

[21] C. Rudin, "Stop explaining black box machine learning models for high stakes decisions and use interpretable models instead," *Nature Machine Intelligence*, vol. 1, no. 5, pp. 206-215, 2019. https://doi.org/10.1038/s42256-019-0048-x

[22] H. Greenspan, B. van Ginneken, and R. M. Summers, "Guest editorial deep learning in medical imaging: Overview and future promise of an exciting new technique," *IEEE Transactions on Medical Imaging*, vol. 35, no. 5, pp. 1153-1159, 2016. https://doi.org/10.1109/TMI.2016.2553401

[23] A. Criminisi, J. Shotton, and E. Konukoglu, "Decision forests: A unified framework for classification, regression, density estimation, manifold learning and semi-supervised learning," *Foundations and Trends in Computer Graphics and Vision*, vol. 7, no. 2-3, pp. 81-227, 2012. https://doi.org/10.1561/0600000035

[24] A. Kumawat and S. Panda, "A robust edge detection algorithm based on feature-based image registration (FBIR) using improved canny with fuzzy logic (ICWFL)," *The Visual Computer*, vol. 38, no. 11, pp. 3681-3702, 2022. https://doi.org/10.1007/s00371-021-02196-1

[25] Y. Duan *et al.*, "Optimizing semi-supervised medical image segmentation with imbalanced filtering and nnU-Net enhancement," *The Visual Computer*, vol. 41, no. 8, pp. 5905-5917, 2025. https://doi.org/10.1007/s00371-024-03759-8

[26] L. Wang, L. He, A. Mishra, and C. Li, "Active contours driven by local Gaussian distribution fitting energy," *Signal Processing*, vol. 89, no. 12, pp. 2435-2447, 2009. https://doi.org/10.1016/j.sigpro.2009.03.014

[27] H.-X. Liu, J.-X. Fang, Z.-J. Zhang, and Y.-C. Lin, "Localised edge-region-based active contour for medical image segmentation," *IET Image Processing*, vol. 15, no. 7, pp. 1567-1582, 2021. https://doi.org/10.1049/ipr2.12126